Kinetics of the Multichannel Reaction of Methanethiyl Radical (CH$_3$S$^\bullet$) with ^{3}O$_2$[†]

Li Zhu and Joseph W. Bozzelli*

Department of Chemistry and Environmental Science, New Jersey Institute of Technology, Newark, New Jersey 07102

The CH$_3$S$^\bullet$ + O$_2$ reaction system is considered an important process in atmospheric chemistry and in combustion as a pathway for the exothermic conversion of methane-thiyl radical, CH$_3$S$^\bullet$. Several density functional and ab initio computational methods are used in this study to determine thermochemical parameters, reaction paths, and kinetic barriers in the CH$_3$S$^\bullet$ + O$_2$ reaction system. The data are also used to evaluate feasibility of the DFT methods for higher molecular weight oxy−sulfur hydrocarbons, where sulfur presents added complexity from its many valence states. The methods include: B3LYP/6-311++G(d,p), B3LYP/6-311++G(3df,2p), CCSD(T)/6-311G(d,p)//MP2/6-31G(d,p), B3P86/6-311G(2d,2p)//B3P86/6-31G(d), B3PW91/6-311++G(3df,2p), G3MP2, and CBS-QB3. The well depth for the CH$_3$S$^\bullet$ + ^{3}O$_2$ reaction to the *syn*-CH$_3$SOO$^\bullet$ adduct is found to be 9.7 kcal/mol. Low barrier exit channels from the *syn*-CH$_3$SOO$^\bullet$ adduct include: CH$_2$S + HO$_2$, (TS6, E_a is 12.5 kcal/mol), CH$_3$ + SO$_2$ via CH$_3$SO$_2$ (TS2′, E_a is 17.8) and CH$_3$SO + O (TS17, E_a is 24.7) where the activation energy is relative to the *syn*-CH$_3$SOO$^\bullet$ stabilized adduct. The transition state (TS5) for formation of the CH$_3$SOO adduct from CH$_3$S$^\bullet$ + O$_2$ and the reverse dissociation of CH$_3$SOO to CH$_3$S$^\bullet$ + O$_2$ is relatively tight compared to typical association and simple bond dissociation reactions; this is a result of the very weak interaction. Reverse reaction is the dominant dissociation path due to enthalpy and entropy considerations. The rate constants from the chemical activation reaction and from the stabilized adduct to these products are estimated as functions of temperature and pressure. Our forward rate constant and CH$_3$S loss profile are in agreement with the experiments under similar conditions. Of the methods above, the G3MP2 and CBS-QB3 composite methods are recommended for thermochemical determinations on these carbon−sulfur−oxygen systems, when they are feasible.

1. Introduction

Oxidation of small sulfur compounds resulting from algae production are considered a source of sulfate production in marine aerosols and cloud condensation nuclei and thus, may play a role in climate regulation.[1] The S−H bonds in alkanethiols CH$_3$SH and CH$_3$CH$_2$SH are 87.5 and 87.6 kcal/mol, respectively, and are weaker than the C−H bond which is 94.2 kcal/mol; thus the thiyl radical is a significant product in the initial reactions of thiols (also named mercaptans).[2] The CH$_3$S$^\bullet$ + O$_2$ reaction is potentially important for both combustion and atmospheric chemistry as a pathway for the exothermic conversion (oxidation) of methanethiyl radical, CH$_3$S$^\bullet$, and as a model reaction for other alkyl thiyl radicals. The presence of sulfur in oxyhydrocarbon systems presents added complexity in studies on thermochemical and kinetic parameters because it can have several valence states.

There are a number of experimental studies in the literature on the reaction of CH$_3$S$^\bullet$ with O$_2$;[2−5] and there is one literature review by Tyndall and Ravishankara[6] on this system. The reaction of CH$_3$S$^\bullet$ with ^{3}O$_2$ is reported to be slow with a rate constant to products (other than to the methane−thiyl−peroxy adduct, CH$_3$SOO$^\bullet$) measured by Tyndall and Ravishankara in 1989 as having an upper limit value of ∼2.5 × 10^{-18} cm^3 molecule^{-1} s^{-1} at 298 K.[3] In 1992, they revisited the system and reported a k of ∼ 4 × 10^{-17} cm^3 molecule^{-1} s^{-1} where the

rate specifically refers to reaction through the CH$_3$SOO$^\bullet$ adduct to new products.[2] The rate constant of CH$_3$S + O$_2$ → CH$_3$SOO was measured as (7−18) × 10^{-14} cm^3 molecule^{-1} s^{-1}. The well depth for CH$_3$S + O$_2$ → CH$_3$SOO was determined at 11.7 ± 0.9 kcal/mol at 298 K, with ΔS for the reaction reported to be −32.2 ± 2.8 and −36.8 ± 2.6 cal/mol·s from second and third law methods of analysis. The equilibrium constant for the reaction is also reported as (1.62 to 79.9) × 10^{-18} cm^3 molecule^{-1} (measurements at 216 to 258 K in 60−80 Torr of He).[2] This shallow well, 11.7 kcal/mol, combined with a small entropy gain from the adduct to the TS structure for dissociation to CH$_3$S$^\bullet$ + O$_2$, results in an adduct lifetime on the order of a microsecond at room temperature.

There are two experimental studies on the dissociation of methylsulfonyl radical (CH$_3$S$^\bullet$(=O)$_2$, where both implicate CH$_3$SOO as a product, one by Butkovskaya and Barnes[7] and one by Frank and Turecek.[8] (for brevity, CH$_3$S$^\bullet$(=O)$_2$ is abbreviated here and in the remaining text as CH$_3$SO$_2$). Butkovskaya and Barnes[7] measured the decay of methyl methanethio-sulfonate (MMTS, CH$_3$S(=O)$_2$SCH$_3$), which resulted in CH$_3$SO$_2$ + CH$_3$S$^\bullet$ in both N$_2$ and O$_2$ at 1 atm. In O$_2$ the CH$_3$S$^\bullet$ reacted to form CH$_3$SOO. They derived rate constants for (CH$_3$SO$_2$ → CH$_3$ + SO$_2$) of 0.4 ± 0.2 s^{-1}, and for (CH$_3$SOO → CH$_3$ + SO$_2$) = 8 s^{-1}, and an equilibrium constant, k_{eq}(CH$_3$S + O$_2$ → CH$_3$SOO) = 1.4 × 10^{-19} cm^3 molecule^{-1} at 298 K. Frank and Turecek[8] studied the dissociation of CH$_3$SO$_2$ and methoxysulfinyl (CH$_3$OSO$^\bullet$ radical, including *anti*- and *syn*-isomers) and ions by variable-time neutralization-reionization mass spectrometry, combined with fast-beam laser photoexci-

---

* Corresponding author. Telephone: (973) 596-5294. Fax: (973) 596-3586. E-mail: bozzelli@adm.njit.edu.

tation experiments. Their studies also included DFT (B3LYP/6-31+G(2d,p)) and ab initio calculations (G2(PMP2)), and RRKM kinetic analysis. They reported $\Delta H_f°_{298}$ for CH_3SO_2 and $CH_3OSO•$ radicals as -50.4 ± 1 and -55.0 ± 1 kcal/mol, respectively. Transition states for CH_3SO_2 dissociation to $CH_3 + SO_2$ and isomerization to *anti*-$CH_3OSO•$ were reported with barriers of 14.3 and 23.4 kcal/mol at the G2(PMP2) level, respectively. The rate constant of CH_3 addition to SO_2 was fitted as log $A = 12.19$ and $E_a = 1.3$ kcal/mol.

The reaction of $CH_3S + O_2$ is also reported as an important submechanism to the detailed model development on photo-oxidation and combustion of dimethyl sulfide and dimethyl disulfide.[9] The rate constants of 5.8×10^{-17} and 600 (both in cm^3 $molecule^{-1}s^{-1}$) for $CH_3S + O_2 + M \rightarrow CH_3SOO• + M$ and reverse $CH_3SOO• + M \rightarrow CH_3S + O_2 + M$ are in this mechanism.

In this study we present thermochemical properties of major species, adducts, TS structures and kinetics for the $CH_3S + O_2$ system. Results from computational studies at several levels are compared to evaluate reasonable calculation methods for thermochemistry and kinetic parameters on larger oxy−hydrocarbon−sulfur systems. Kinetic parameters, equilibrium constant, and CH_3S loss profiles are compared with the literature data.

2. Methods

The reactants, intermediates, products, and transition state structures resulting from the $CH_3S• + {}^3O_2$ association reaction are calculated at several density functional and composite ab initio levels using Gaussian 03. Computation levels include B3LYP/6-311++G(d,p), B3LYP/6-311++G(3df,2p), CCSD(T)/6-311G(d,p)//MP2/6-31G(d,p), B3P86/6-311G(2d,2p)//B3P86/6-31G(d), and B3PW91/6-311++G(3df,2p). Zero point energies are corrected by 0.9806 (both B3LYP methods), 0.9608, 0.9759, and 0.9774 for MP2/6-31G(d,p), B3P86/6-31G(d), and B3PW91/6-311++G(3df,2p) methods, respectively. The CBS-QB3 and G3MP2 composite methods are utilized for improved energies and analysis. G2 and G3 are applied when the CBS-QB3 and G3MP2 do not agree.

The enthalpies of formation for stable species (non-TS's, Table 3 of the previous article[10]) are calculated using the total energies at B3LYP/6-311++G(d,p), B3LYP/6-311++G(3df,2p), and CBS-QB3 levels with work reactions that are isodesmic in most cases. Isodesmic reactions conserve the number and type of bonds on both sides of an equation. The use of a work reaction with similar bonding on both sides of a equation, results in a cancellation of calculation error and improves the accuracy for energy analysis. The reported enthalpy values can be compared with the known enthalpies of several molecules in the system to serve as a calibration on the thermochemistry and the PE diagram.

The energy of each transition state structure is calculated from the corresponding reactant plus the energy difference between the TS structure and the reactant (adduct). If the TS is closer in structure to the product, then the enthalpies of formation of the transition state species is calculated from the corresponding product plus the energy difference between TS and product.

Contributions to $S°_{298}$ and $C_p°(T)$ of each species and TS structure are calculated using the "SMCPS" program,[11] which incorporates the frequencies, moments of inertia, mass, symmetry, number of optical isomers, from the CBS-QB3 or G3MP2 Gaussian calculation. It also incorporates frequency corrections. Torsion frequencies are omitted in SMCPS, and the

"ROTATOR" program[11−13] is used for contributions from internal rotations to $S°_{298}$ and $C_p°(T)$.

The rate constants for the elementary reactions are calculated from the computed frequencies, structures and energies using canonical transition state theory with rate $k(T)$ fit to the three-parameter modified Arrhenius equation, $k = A \times T^n \times \exp(-E_a/RT)$, over the temperature range 237−2000 K.[11,14] The calculation of the preexponential term $A \times T^n$ uses all vibration frequencies, but torsion frequencies are omitted. In place of the torsion frequency the internal rotor potentials are analyzed and their contributions to entropy and heat capacity are included.

Temperature and pressure dependent rate constants for reactions of the chemical activated CH_3SOO* and the stabilized CH_3SOO adduct were calculated with multichannel, multi-frequency QRRK theory for $k(E)$ and master equation analysis for falloff.[11] Elementary rate constants for the individual reaction, preexponential factors and the energies were obtained from canonical transition state theory. The CHEMASTER[11] code is used with energy levels from a full set of 3N-6 vibration frequencies, but in a reduced form of three representative frequency sets, plus energy levels from one external rotor.

The CHEMKIN II program[15] is used to integrate the kinetics for the $CH_3S + O_2$ mechanism; it incorporates thermodynamic properties and microscopic reversibility to determine the reverse rate constants, which are then included in the model. The reaction conditions are taken as the experimental conditions of Turnipseed et al.,[2] and the modeling results are compared with the experiment.

3. Results and Discussion

The potential energy diagram for the CH_3S radical with O_2 reaction system is illustrated in Figure 1. Values are standard enthalpy of formation at 298 K. The thermochemical properties for atoms, diatomics, HO_2, SO_2, CH_3, CH_3S, CH_2O, CH_3O, and ^3SO, are from the literature. All other intermediates including CH_3SO_2 are from calculations with isodesmic work reactions.[10] The values for the transition states are calculated from the difference in the enthalpies of formation of reactants and the corresponding barriers, except TS5 which is calculated from product, *anti*-CH_3SOO (using the reverse barrier height). Enthalpy values for transition states are at G3MP2 level except those marked with ∗ or ∗∗, which are at the CBS-QB3 or G2 levels, respectively. The thermochemical properties are listed in Table 3 and some of the $\Delta H_f°_{298}$ data are derived in a previous study.[10] The potential energy diagram in Figure 1 includes a number of paths that do not show importance to the forward reaction of the $CH_3S + O_2$ system; these paths have value in reaction systems such as $CH_3O + SO$, $CH_2O + HSO$ (or SOH), $CH_3 + SO_2$ and will be further discussed in future studies.

The association of CH_3S with O_2 forms an energized adduct, *anti*-CH_3SOO* (dihedral angle $\angle CSOO = 179°$ at CBS-QB3 level) with 9.2 kcal/mol of energy; $\Delta H_f°_{298}$ of the *anti*-CH_3SOO adduct, 20.7 kcal/mol, is determined by reference to the *syn*-CH_3SOO.[10] The energy of the transition state structure for the $CH_3S + O_2$ association (TS5) is determined relative to the CH_3SOO adduct and is approximately 5.0 kcal/mol below the entrance channel of the reactants. We treat the $CH_3S + O_2$ reaction to TS5 as having no E_a and TS5 at the energy of the reactants. The reactant's energies for CH_3S are from literature, which is supported by work reaction calculation, and from the definition, $\Delta H_f°_{(298)}$, for $^3O_2$.

The CH_3SOO adducts (energized and stabilized) can isomerize via several processes; these include internal rotation about

Multichannel Reaction of Methanethiyl Radical

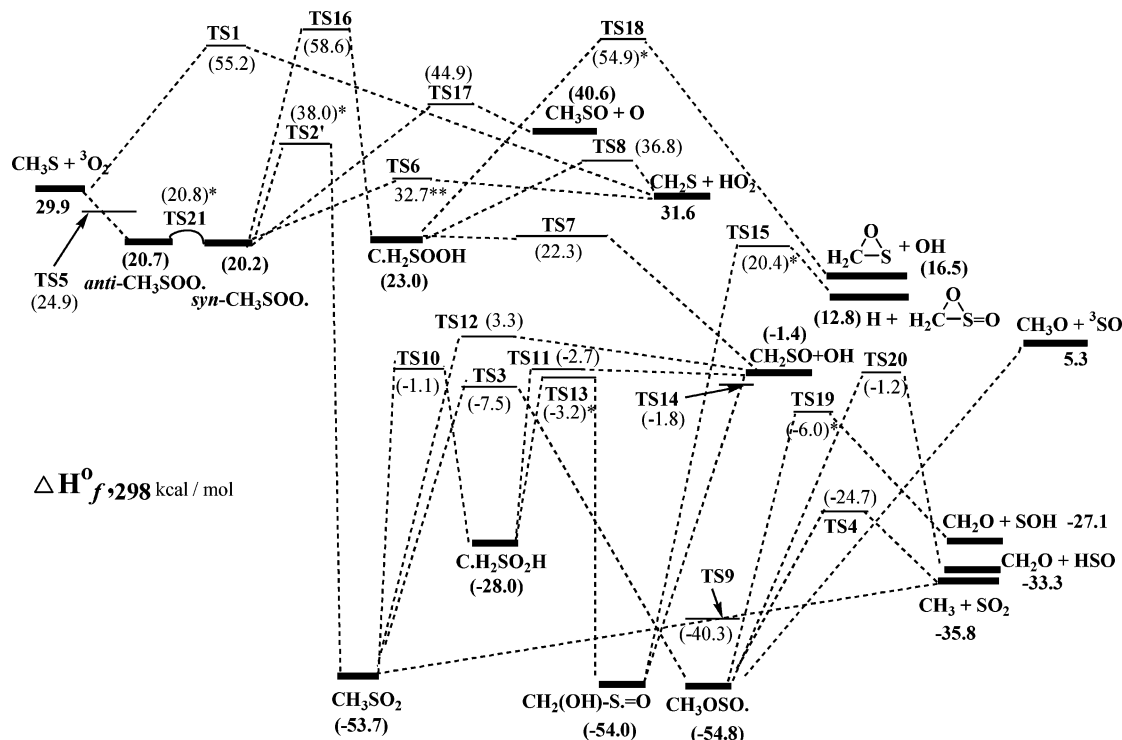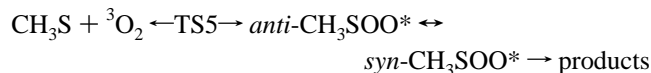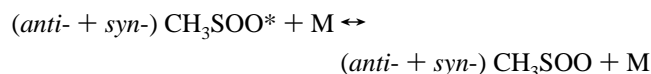*J. Phys. Chem. A, Vol. 110, No. 21, 2006* **6925**

Figure 1. Potential energy diagram at 298 K (in kcal/mol). All barriers are calculated at G3MP2 level, except those labeled with an asterisk are calculated in CBS-QB3 level. TS6 with two asterisks is from the G2 calculation. Energy of TS5 is treated as being at the energy of the $CH_3S + O_2$ reactants.

CH_3S-OO, H atom transfer, rearrangement of the $(S-O-O)$ moiety, and dissociation back to reactants.

The TS5 structure suggests that the CH_3SOO* is formed in the *anti*-form, and the reaction path analysis indicates that H transfer reactions and HO_2 molecular elimination paths occur from the *syn*-form.
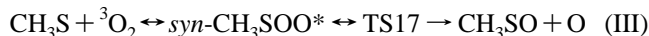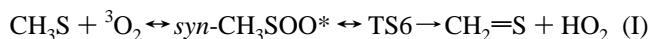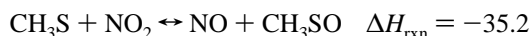
$$CH_3S + {}^3O_2 \leftarrow TS5 \rightarrow anti\text{-}CH_3SOO* \leftrightarrow$$
$$syn\text{-}CH_3SOO* \rightarrow \text{products}$$

and

$$(anti\text{-} + syn\text{-})\, CH_3SOO* + M \leftrightarrow$$
$$(anti\text{-} + syn\text{-})\, CH_3SOO + M$$
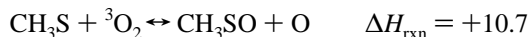
The *anti*-CH_3SOO undergoes an internal rotation with a barrier of only 0.1 kcal/mol at 298 K to the *syn*-CH_3SOO (dihedral angle $\angle CSOO = 0°$ at CBS-QB3 level). The *syn*-CH_3SOO is 0.5 kcal/mol more stable than the *anti*-form. The barriers to other isomers or products are all above the energy of the $CH_3S + O_2$ entrance channel.

There are three low-energy forward reaction channels of *syn*-CH_3SOO. The most important at atmospheric conditions is molecular elimination of HO_2 (I) with an E_a of 12.5 kcal/mol and a tight transition state ($A_{298} = \sim 4E+11$) at 298 K via TS6. The peroxy oxygen atom forms a bond with the H atom in a five member ring TS structure, the $S-O$ bond cleaves and the $C=S$ double bond is formed. The second low barrier forward reaction II, is isomerization via attack of the peroxy radical on the S atom (addition, formation of a three member SOO ring) and cleavage of the weak $RO-O$ bond to form a much more stable CH_3SO_2 adduct ($\Delta H_{rxn} = -73.9$) with E_a of 17.8 kcal/mol and a tight transition state ($A_{298} = \sim 5E+11$). The third important unimolecular reaction is CH_3SO-O bond cleavage to $CH_3SO + O$ via TS17 (III) with E_a of 24.7 kcal/mol; but a somewhat less tight transition state ($A_{298} = \sim 7E+12$). This channel will be more important at elevated temperatures.

$$CH_3S + {}^3O_2 \leftrightarrow syn\text{-}CH_3SOO* \leftrightarrow TS6 \rightarrow CH_2{=}S + HO_2 \quad (I)$$

$$CH_3S + {}^3O_2 \leftrightarrow syn\text{-}CH_3SOO* \leftrightarrow TS2' \rightarrow CH_3 + SO_2 \quad (II)$$

$$CH_3S + {}^3O_2 \leftrightarrow syn\text{-}CH_3SOO* \leftrightarrow TS17 \rightarrow CH_3SO + O \quad (III)$$

It is interesting to compare the thermochemistry of CH_3 radical with that of CH_3S in overall reactions with O_2 and NO to observe the significant difference in reaction energy resulting from the change in valence of sulfur. We note that CH_3SO exists in the $CH_3S^\bullet(=O)$ resonant form.

$$CH_3 + {}^3O_2 \leftrightarrow CH_3O + O \qquad \Delta H_{rxn} = +29.8 \text{ kcal/mol}$$

$$CH_3S + {}^3O_2 \leftrightarrow CH_3SO + O \qquad \Delta H_{rxn} = +10.7$$

$$CH_3 + NO_2 \leftrightarrow NO + CH_3O \qquad \Delta H_{rxn} = -16.4$$

$$CH_3S + NO_2 \leftrightarrow NO + CH_3SO \qquad \Delta H_{rxn} = -35.2$$

3.1. Comparison of Enthalpy and Reaction Barriers vs Level of Theory and Basis Set. Our previous study on thermochemistry of carbon–sulfur–oxygen species[10] showed that use of larger basis sets with the B3LYP calculations and work reaction analysis resulted in improved accuracy. The B3LYP/ 6-311++G(3df,2p) level was, however, still not sufficiently accurate to be in agreement with the accepted literature or G3MP2 data for approximately 20 percent of the reactions. The B3PW91/6-311++G(3df,2p) calculation level showed similar accuracy to the B3LYP/6-311++G(3df,2p) and these were judged as the best in this DFT comparison. The CCSD(T)/6-311G(d,p)//MP2/6-31G(d,p) calculations (with work reactions), were not as accurate as the best DFT level calculation sets. The B3P86/6-311G(2d,2p)//B3P86/6-31G(d) level performed in a manner similar to the B3LYP/6-311++G(d,p). Overall, we concluded that the results from the work reactions and these DFT methods were not consistently satisfactory or

TABLE 1: Comparison of E_a (Forward or Reverse) at Different Calculation Levels[a,b]

	B3LYP I[c]	B3LYP II[d]	CCSD(T)/ 6-311G(d,p)// MP2/6-31G(d,p)	B3P86/ 6-311G(2d,2p)// B3P86/ 6-31G(d)	B3PW91/ 6-311++G(3df,2p)	CBS-QB3	G3MP2	G3MP2 (0 K, ref 16)	G2(PMP2) (0 K, ref 8)
$CH_3S + O_2 \rightarrow TS1$	20.6	20.3	29.3	26.2	20.3	24.3	25.3	11.2	
$syn\text{-}CH_3SOO \rightarrow TS2'$	30.6	22.8	33.6	27.1	23.2	17.8		18.6	
$CH_3SO_2 \rightarrow TS3$	39.9	45.0	47.8	45.5	47.4	48.1	46.2	49.4	23.4[g]
$CH_3OSO \rightarrow TS4$	31.9	27.6	38.5	30.0	29.1	28.6	30.1	30.9	36.3[g]
$TS5 \rightarrow syn\text{-}CH_3SOO$[e]	4.8	7.0	8.4		8.3	6.6	4.7	8.3	
$syn\text{-}CH_3SOO \rightarrow TS6$[f]	13.2	14.2	11.9	11.8	13.4	13.1	9.9		
$C^\bullet H_2SOOH \rightarrow TS7$	−0.5	−0.7	3.4	−0.4	−2.0	−1.1	−0.7	1.0	
$C^\bullet H_2SOOH \rightarrow TS8$	3.6	8.8	7.8	7.3	8.8	7.0	13.8	13.4	
$CH_3SO_2 \rightarrow TS9$			13.0				13.4	14.4	14.3
$CH_3SO_2 \rightarrow TS10$	45.6	51.8	46.5	48.6	51.4	53.8	52.6		
$C^\bullet H_2SO_2H \rightarrow TS11$				32.2	34.2	36.8	25.3		
$CH_3SO_2 \rightarrow TS12$	54.1	56.9	57.5	53.7	55.4	56.2	57.0		
$C^\bullet H_2SO_2H \rightarrow TS13$	14.4	20.4	19.6	21.3	23.2	24.8			
$CH_2(OH)S^\bullet\!=\!O \rightarrow TS14$	53.8		54.5	55.4	53.5	52.3	52.2		
$CH_2(OH)S^\bullet\!=\!O \rightarrow TS15$	81.4	75.3	84.0	77.4	74.0	74.4			
$syn\text{-}CH_3SOO \rightarrow TS16$		35.3	37.6	34.5	34.3		38.4	39.6	
$syn\text{-}CH_3SOO \rightarrow TS17$							24.7		
$C^\bullet H_2SOOH \rightarrow TS18$	26.0	27.0	32.2	30.5	27.9	31.9			
$CH_3OSO \rightarrow TS19$						48.8			
$CH_3OSO \rightarrow TS20$							53.6		
$anit\text{-}CH_3SOO \rightarrow TS21$						0.07			

[a] Units in kcal/mol, at 298 K. [b] See Figure 1 for an illustration of the transition states. [c] B3LYP I = B3LYP/6-311++G(d,p). [d] B3LYP II = B3LYP/6-311++G(3df,2p). [e] TS5 is the transition state for $CH_3S + O_2 \rightarrow syn\text{-}CH_3SOO$, The vales here are E_a for the reverse reaction to the TS5. [f] TS6 is calculated at 12.5 at G2 and 12.4 at G3 levels of calculation. [g] This is for *anti*-CH_3OSO, which is 2.2 kcal/mol higher in energy than the *syn*- form at G2(PMP2).

were too dependent on the work reaction. We observed that the two composite methods, CBS-QB3 and G3MP2 yielded the best results compared to experiment and these calculation methods are recommended for this carbon−sulfur−oxygen system.

Reaction barriers from three DFT methods (B3LYP, B3P86, and B3PW91) using several basis sets, along with two composite methods CBS-QB3 and G3MP2 are compared in Table 1 for most of the 21 transition state structures. Data on several reactions from studies by Frank and Turecek and by Wang et al. are also listed. Energy values in Table 1 are activation energies at 298 K calculated from the relative total energies between TS and reactants (except TS5, which is between TS and products). The following discussion addresses some of the data in Table 1.

There is reasonable agreement (within 2 kcal/mol) for the energies of activation between the CBS-QB3 and G3MP2 calculation methods, in 8 out of 11 reactions (see Table 1). Possible reasons for the varied results from the different calculation methods and basis sets include the following: (1) differences in geometry that arise from use of different methods and basis sets; (2) varied treatment of the multivalence complexity of the S atom by the methods (the S atom can have four different valence states); (3) improvements in the composite methods resulting from techniques to extend the basis function energies to those of a complete or a more complete basis set. For the density functional methods, the data in Table 1 show that the higher-level B3LYP and the B3PW91 have better agreement with the composite methods a majority of the time.

A 3.2 kcal/mol difference is observed between CBS-QB3 and G3MP2 calculations for TS6 (see Table 1), where TS6 represents HO_2 molecular elimination from the $CH_3SOO^\bullet$ adduct with a low barrier. It is an important path because it controls the product set from unimolecular reaction of the CH_3SOO adduct at low temperatures and it may explain the reaction path observed in the low-temperature flow experiments of Turnipseed et al.[2] The CBS-QB3 and G3MP2 structure calculations result in different r65 and r51 atom distances in the TS6 transition state structure (see Table 2). The breaking r51 bond is 1.447

and 1.279 Å, and the forming r65 bond is 1.178 and 1.357 Å, at CBS-QB3 and G3MP2 levels, respectively. We performed higher-level calculations on this TS-structure at the G3 and G2 level because of the importance of this channel; these results show good agreement at 12.5 and 12.4 kcal/mol respectively, and are in moderate agreement with the CBS-QB3 data at 13.1 kcal/mol. We choose the G2 value for use in our kinetic analysis.

The difference in calculated values for TS11 by CBS-QB3 and G3MP2 is 11.2 kcal/mol; with values of 25.3 at G3MP2 and 36.8 at CBS-QB3. Here we observe that the r31 and r41 bond lengths and the ∠412 plus ∠541 bond angles in TS11 are significantly different at the two levels. The bond length of r31 is 1.531 and 1.496 Å, and r41 is 2.017 and 2.404 Å, at CBS-QB3 and G3MP2 levels, respectively. The bond angles of ∠412 are 111 and 94°, and the ∠541 are 108 and 94°, at CBS-QB3 and G3MP2 levels, respectively. We choose the CBS-QB3 value based on our evaluation that the reverse reaction, OH addition to the S, does not have a 11 kcal/mol barrier, and further note that reaction through TS11 is unimportant in this $CH_3S + O_2$ system.

One additional barrier where the CBS-QB3 and G3MP2 calculations result in different values is TS8, where the structures are also different at the two levels (Table 2). The activation energy to TS8 is 7.0 kcal/mol at CBS-QB3 vs 13.8 kcal/mol at G3MP2:

$$C^\bullet H_2SOOH\ (TS8) \rightarrow CH_2S + HO_2$$
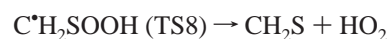
The barrier height of TS8 is relatively unimportant in the forward direction, because $C^\bullet H_2SOOH$ rapidly dissociates to lower energy products $CH_2SO + OH$ via TS7 with no barrier. It is also difficult for the initial CH_3SOO adduct to reach the $C^\bullet H_2SOOH$ adduct because the conversion of $CH_3SOO^\bullet$ to $C^\bullet H_2SOOH$ has a barrier (TS16) of 38.4 kcal/mol.

There is a difference of 14.1 kcal/mol between our data and those of Wang et al.[16] for the abstraction of a methyl H atom by O_2, at the same G3MP2 level. We note that the TS structure

Multichannel Reaction of Methanethiyl Radical

J. Phys. Chem. A, Vol. 110, No. 21, 2006 **6927**

TABLE 2: Geometries and (Imaginary) Vibrational Frequencies of Intermediates and TS[a–c]

		Bond length (Angstrom)		Bond angle (degree)		Dihedral angle (degree)	
anti- CH₃SOO	R21	1.093					
	R31	1.090	--	∠312	109	--	
	R41	1.090	--	∠412	109	--	∠4123	-122	--
	R51	1.804	--	∠512	105	--	∠5123	119	--
	R65	1.831	--	∠651	94	--	∠6512	178	--
	R76	1.282	--	∠765	115	--	∠7651	179	--
		63	--				

syn- CH₃SOO	R21	1.090	--				
	R31	1.089	--	∠312	112	--	
	R41	1.103	--	∠412	109	--	∠4123	-120	--
	R51	1.787	--	∠512	111	--	∠5123	125	--
	R65	1.921	--	∠651	98	--	∠6512	117	--
	R76	1.261	--	∠765	117	--	∠7651	0	--
		126	--				

CH₃SO₂	R21	1.088	1.089				
	R31	1.090	1.092	∠312	111	111	
	R41	1.088	1.089	∠412	112	112	∠4123	-126	-124
	R51	1.836	1.809	∠512	108	108	∠5123	116	117
	R65	1.466	1.481	∠651	107	107	∠6512	175	174
	R75	1.466	1.481	∠751	107	107	∠7512	-54	-53
		152	197				

CH₃OSO	R21	1.089	1.088				
	R31	1.091	1.090	∠312	110	111	
	R41	1.094	1.092	∠412	110	110	∠4123	-121	-121
	R51	1.442	1.446	∠512	106	105	∠5123	120	119
	R65	1.662	1.657	∠651	118	115	∠6512	-169	-176
	R76	1.482	1.483	∠765	111	112	∠7651	31	13
		65	90				

C.H₂SOOH	R21	1.082	1.073				
	R31	1.082	1.073	∠312	121	121	
	R41	1.679	1.725	∠412	118	118	∠4123	-180	167
	R54	1.691	1.655	∠541	104	101	∠5412	147	156
	R65	1.487	1.399	∠654	112	112	∠6541	-79	-79
	R76	0.968	0.951	∠765	100	102	∠7654	-101	-101
		121	132				

C.H₂SO₂H	R21	1.083	1.083				
	R31	1.084	1.083	∠312	123	121	
	R41	1.755	1.756	∠412	119	119	∠4123	-170	-165
	R54	1.473	1.487	∠541	105	106	∠5412	168	-169
	R64	1.692	1.681	∠641	98	96	∠6412	-78	-55
	R76	0.971	0.983	∠764	108	108	∠7641	-59	-62
		125	132				

CH₂OHS.=O	R21	1.092	1.100				
	R31	1.099	1.093	∠312	110	110	
	R41	1.873	1.844	∠412	108	107	∠4123	-115	-118
	R54	1.521	1.497	∠541	101	101	∠5412	-149	-93
	R61	1.387	1.392	∠612	110	113	∠6123	126	123
	R76	0.972	0.986	∠761	107	105	∠7612	153	85
		92	82				

TABLE 2 (Continued)
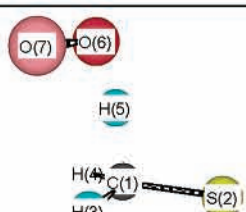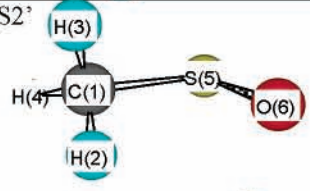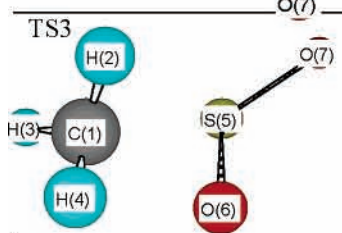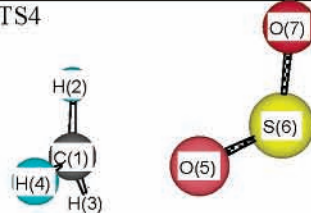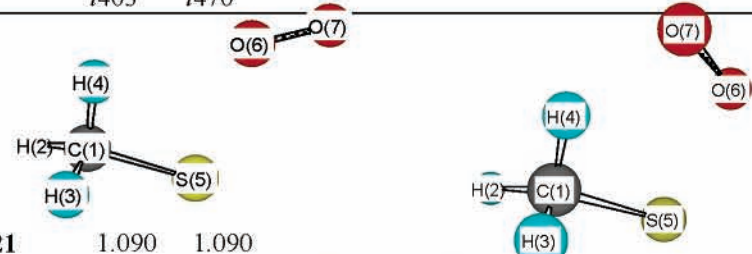
		Bond length (Angstrom)		Bond angle (degree)			Dihedral angle (degree)		
TS1	R21	1.680	1.674						
	R31	1.094	1.095	∠312	119	120			
	R41	1.092	1.091	∠412	119	119	∠4123	-148	-150
	R51	1.334	1.356	∠512	105	105	∠5123	103	99
	R65	1.252	1.208	∠651	170	161	∠6512	-171	-155
	R76	1.250	1.247	∠765	113	110	∠7651	30	26
		i2102	i3706						
TS2'	R21	1.089	--						
	R31	1.091	--	∠312	111	--			
	R41	1.092	--	∠412	111	--	∠4123	-123	--
	R51	1.809	--	∠512	106	--	∠5123	120	--
	R65	1.547	--	∠651	104	--	∠6512	-43	--
	R76	1.755	--	∠765	75	--	∠7651	90	--
		i832	--						
TS3	R21	1.083	1.088						
	R31	1.085	1.088	∠312	116	111			
	R41	1.081	1.092	∠412	115	113	∠4123	-137	-124
	R51	2.313	2.060	∠512	94	98	∠5123	92	101
	R65	1.582	1.585	∠651	57	58	∠6512	114	130
	R75	1.465	1.482	∠751	130	116	∠7512	20	24
		i1004	i139						
TS3 (Frank and Turecek)[8] B3LYP/6-31+G(2d,p)	R21	1.082							
	R31	1.082		∠312	120				
	R41	1.081		∠412	119				
	R51	2.350		∠512	88				
	R65	1.496		∠651	35				
	R75	1.480		∠751	104				
		i251							
TS4	R21	1.080	1.080						
	R31	1.080	1.081	∠312	119	118			
	R41	1.079	1.079	∠412	119	118	∠4123	-158	-153
	R51	2.152	2.055	∠512	98	98	∠5123	103	106
	R65	1.488	1.457	∠651	122	124	∠6512	-50	-63
	R76	1.461	1.448	∠765	117	120	∠7651	75	78
		i403	i470						
TS5	R21	1.090	1.090						
	R31	1.090	1.090	∠312	111	111			
	R41	1.095	1.106	∠412	108	108	∠4123	-119	-119
	R51	1.808	1.774	∠512	111	112	∠5123	124	125
	R65	2.314	2.032	∠651	90	94	∠6512	118	117
	R76	1.214	1.219	∠765	120	117	∠7651	-180	0
		i115	i776						

TABLE 2 (Continued)
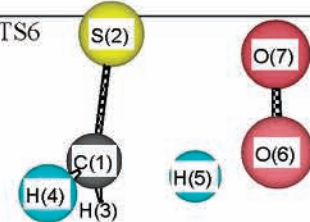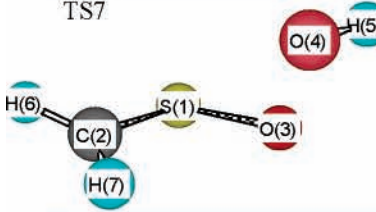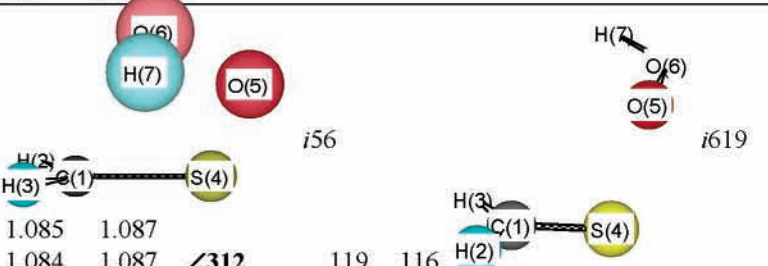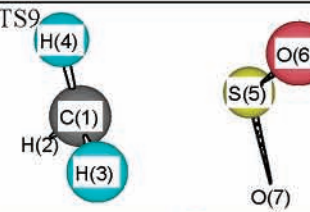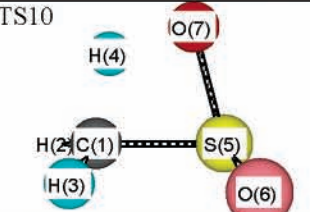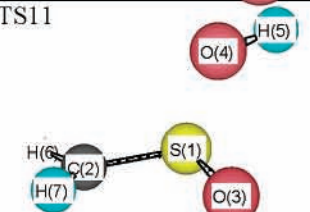
		Bond length (Angstrom)		Bond angle (degree)			Dihedral angle (degree)	
TS6	R21	1.660	1.678					
	R31	1.090	1.088	∠312	120	117		
	R41	1.090	1.088	∠412	120	117	∠4123	-155	-143
	R51	1.447	1.279	∠512	93	95	∠5123	103	109
	R65	1.178	1.357	∠651	155	146	∠6512	0	0
	R76	1.265	1.262	∠765	102	97	∠7651	0	0
		*i*990	*i*3596					
TS7	R21	1.676	1.662					
	R31	1.618	1.540	∠312	106	108		
	R43	1.595	1.652	∠431	112	113	∠4312	-83	-84
	R54	0.968	0.976	∠543	96	95	∠5431	-116	-122
	R62	1.082	1.081	∠621	118	118	∠6213	158	169
	R72	1.082	1.081	∠721	120	121	∠7213	-22	-12
		*i*458	*i*971					
TS8					*i*56				*i*619
	R21	1.085	1.087					
	R31	1.084	1.087	∠312	119	116		
	R41	1.629	1.622	∠412	120	122	∠4123	-174	178
	R54	1.926	2.074	∠541	108	105	∠5412	131	-107
	R65	1.413	1.372	∠654	111	114	∠6541	-6	-98
	R76	0.968	0.980	∠765	102	103	∠7654	107	97
TS9	R21	--	1.083					
	R31	--	1.084	∠312	--	117		
	R41	--	1.083	∠412	--	118	∠4123	--	-148
	R51	--	2.361	∠512	--	101	∠5123	--	103
	R65	--	1.472	∠651	--	100	∠6512	--	179
	R75	--	1.472	∠751	--	100	∠7512	--	-58
		--	*i*315					
TS10	R21	1.085	1.086					
	R31	1.087	1.089	∠312	121	120		
	R41	1.344	1.315	∠412	109	108	∠4123	-126	-124
	R51	1.811	1.789	∠512	117	117	∠5123	144	143
	R65	1.465	1.481	∠651	108	108	∠6512	-151	-150
	R74	1.239	1.251	∠741	114	110	∠7412	-108	-107
		*i*1951	*i*2971					
TS11	R21	1.613	1.601					
	R31	1.531	1.496	∠312	108	115		
	R41	2.017	2.404	∠412	111	94	∠4123	-83	-120
	R54	0.972	0.981	∠541	108	94	∠5412	-163	-166
	R62	1.083	1.083	∠621	117	117	∠6213	-166	177
	R72	1.082	1.084	∠721	121	122	∠7213	20	-1
		*i*547	*i*442					

TABLE 2 (Continued)
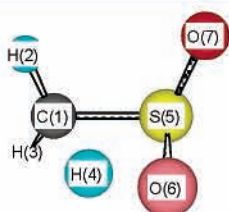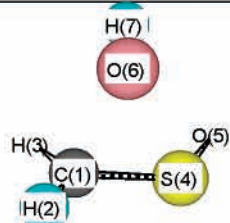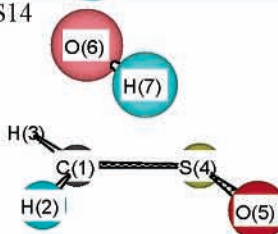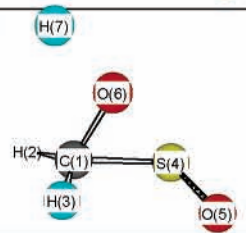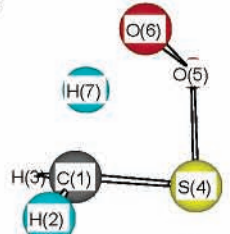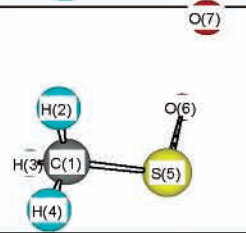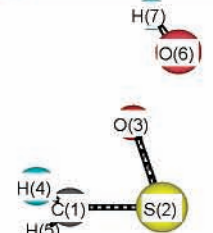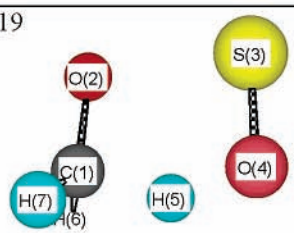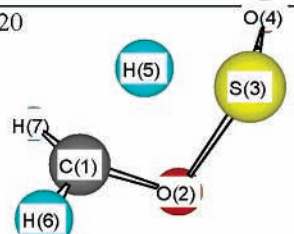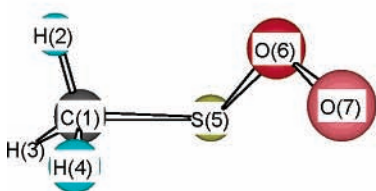
		Bond length (Angstrom)		Bond angle (degree)			Dihedral angle (degree)		
TS12	R21	1.089	1.089						
	R31	1.090	1.090	∠312	113	114			
	R41	1.476	1.494	∠412	131	138	∠4123	-152	-145
	R51	1.789	1.734	∠512	114	115	∠5123	127	131
	R64	1.253	1.267	∠641	122	119	∠6412	-109	-115
	R75	1.469	1.459	∠751	115	118	∠7512	12	17
		i2449	i2038						
TS13	R21	1.081	--						
	R31	1.083	--	∠312	121	--			
	R41	1.648	--	∠412	117	--	∠4123	-175	--
	R54	1.477	--	∠541	112	--	∠5412	176	--
	R61	2.251	--	∠612	92	--	∠6123	113	--
	R76	0.972	--	∠761	94	--	∠7612	-152	--
		i277	i2971						
TS14	R21	1.082	1.082						
	R31	1.084	1.084	∠312	121	120			
	R41	1.620	1.610	∠412	123	122	∠4123	-180	-172
	R54	1.485	1.509	∠541	114	112	∠5412	-4	-11
	R61	2.564	2.297	∠612	71	77	∠6123	107	101
	R76	0.977	0.983	∠761	86	89	∠7612	82	76
		i137	i265						
TS15	R21	1.090	--						
	R31	1.090	--	∠312	116	--			
	R41	1.802	--	∠412	119	--	∠4123	139	--
	R54	1.465	--	∠541	112	--	∠5412	-147	--
	R61	1.412	--	∠612	116	--	∠6123	-142	--
	R76	1.740	--	∠761	113	--	∠7612	62	--
		i799	--						
TS16*	R21	1.085	1.088						
	R31	1.090	1.090	∠312	116	115			
	R41	1.753	1.783	∠412	114	116	∠4123	-140	-140
	R54	1.773	1.730	∠541	88	87	∠5412	-153	-148
	R65	1.400	1.404	∠654	103	103	∠6541	51	49
	R76	1.257	1.244	∠765	94	95	∠7654	-39	-42
		i2759	i3702						
	* = here use B3LYP/6-311++G(2d,p) geom. And freq., CBS-QB3 is not found								
TS17	R21	--	1.091						
	R31	--	1.090	∠312	--	110			
	R41	--	1.093	∠412	--	110	∠4123	--	-121
	R51	--	1.797	∠512	--	109	∠5123	--	121
	R65	--	1.534	∠651	--	104	∠6512	--	-65
	R76	--	1.778	∠765	--	114	∠7651	--	85
		--	i838						
TS18	R21	1.708	--						
	R32	1.698	--	∠321	70	--			
	R41	1.081	--	∠412	118	--	∠4123	-78	--
	R51	1.083	--	∠512	121	--	∠5123	104	--
	R63	1.790	--	∠632	114	--	∠6321	142	--
	R76	0.969	--	∠763	92	--	∠7632	179	--
		i772	--						

TABLE 2 (Continued)

		Bond length (Angstrom)		Bond angle (degree)			Dihedral angle (degree)		
TS19									
	R21	1.283	--						
	R32	1.284	--	∠321	103	--			
	R43	1.538	--	∠432	86	--	∠4321	0	--
	R54	1.244	--	∠543	105	--	∠5432	0	--
	R61	1.102	--	∠612	118	--	∠6123	-105	--
	R71	1.102	--	∠712	118	--	∠7123	105	--
		$i1275$	--						
TS20									
	R21	--	1.396						
	R32	--	1.732	∠321	--	100			
	R43	--	1.481	∠432	--	114	∠4321	--	-96
	R53	--	1.529	∠532	--	76	∠5321	--	10
	R61	--	1.086	∠612	--	114	∠6123	--	-126
	R71	--	1.088	∠712	--	115	∠7123	--	91
		--	$i2314$						
TS21									
	R21	1.090	--						
	R31	1.094	--	∠312	109	--			
	R41	1.089	--	∠412	111	--	∠4123	-121	--
	R51	1.807	--	∠512	111	--	∠5123	115	--
	R65	1.824	--	∠651	96	--	∠6512	56	--
	R76	1.290	--	∠765	115	--	∠7651	112	--
		$i65$	--						

[a] First structure = CBS-QB3 level; second structure = G3MP2 when they are different. [b] First column = CBS-QB3 parameters; second column = G3MP2 parameters. [c] First imaginary frequency = B3LYP in CBS-QB3, second imaginary frequeancy = HF in G3MP2.

for abstraction reaction in Wang et al. is similar to our TS6 (HO$_2$ molecular elimination from CH$_3$SOO) rather than our TS1.[10]

There are three reaction barriers in this system that have been previously reported by Frank and Turecek[8] in their study on the CH$_3$ + SO$_2$ reaction surface. We include their data, which is reported to be at a G2(PMP2) calculation level, in Table 1 for comparison.

One reaction is CH$_3$SO$_2$ → CH$_3$ + SO$_2$ (TS9 in this study), where the barrier by Frank and Turecek is 14.3 kcal/mol, and the value in this work is 13.4 kcal/mol at G3MP2 level. Wang et al.[16] also reported this value as 14.4 kcal/mol at G3MP2 level. The well depth of CH$_3$ + SO$_2$ to CH$_3$SO$_2$ is 14.1 kcal/mol at G2(PMP2) level by Frank and Turecek, but our isodesmic reaction analysis on CH$_3$SO$_2$ radical places this well depth at 17.9 kcal/mol. We feel these differences may be attributed to differences in reference species. We reference the TS to the adduct energy, which is obtained from work reactions. Frank and Turecek may be have referenced the energy to values calculated for the reactants. The Turecek research group has a strong publication record for both enthalpy and kinetic barriers and we regard their work highly.

A second reaction in the Frank and Turecek study is CH$_3$SO$_2$ → CH$_3$OSO (TS3 in this study), and there is a 25 kcal/mol difference between our E_a (48.1 at CBS-QB3 level) and their value (23.4 kcal/mol). Wang et al.[16] also report this TST with a value of 49.4 kcal/mol. The published TS structure by Frank and Turecek (reported as at B3LYP/6-31+G(2d,p) level in their SM) and ours (at B3LYP/6-311G(2d,d,p) in CBS-QB3) are compared in Table 2 (see TS3 section). There are significant differences in the r(C−S), and one of the r(O−S) bond lengths

and the ∠CSO angle. We ran a TS calculation on the geometry of Frank and Turecek using their B3LYP/6-31+G(2d,p) method. The output geometry was similar to the initial; but the IRC analysis suggested the TS may be for CH$_3$OSO → CH$_3$ + SO$_2$ (TS4 in this study) rather than for CH$_3$OSO → CH$_3$SO$_2$ (TS3). We note that our barrier for the CH$_3$OSO → CH$_3$ + SO$_2$ reaction (TS4) is 28.6 kcal/mol at CBS-QB3 and 30.1 kcal/mol at G3MP2. The E_a for TS4 is also reported as 30.9 kcal/mol by Wang et al. These values are more similar to the Frank and Turecek data; but still several kilocalories per mole higher than their E_a of 23.4. We will analyze this further in future work on the CH$_3$ + SO$_2$ reaction system.

Frank and Turecek also calculated the barrier for CH$_3$OSO → CH$_3$ + SO$_2$ (TS4 in this study) and reported the E_a at the G2(PMP2) level, is 36.6 kcal/mol, which is 6 to 8 kcal/mol higher than our CBS-QB3 and G3MP2 results. We have recalculated this TST with their reported B3 geometry and confirm the structure and path analysis are in agreement. The difference in energy may result from reference of the TS energy to the CH$_3$SO$_2$ and CH$_3$OSO adducts in this study, i.e., the work reaction analysis for the ΔH_f values, vs reference of the TS energy to the calculated energy of the CH$_3$ + SO$_2$ reactants by Frank and Turecek.

3.2. Structures of TS and IRC Calculations. The geometries and the imaginary frequencies of the transition state structures from the CBS-QB3 or G3MP2 calculations are listed in Table 2; structures for the two forms of the initial adduct CH$_3$SOO and the intermediates are also included. The geometry and frequencies were calculated in the CBS-QB3 method as CBSB7 or B3LYP/6-311G(2d,d,p). The method for geometry and frequency calculation in G3MP2 is MP2(Full)/6-31G(d) and HF/

TABLE 3: Ideal Gas-Phase Thermochemical Properties[a]

species	$\Delta H_f°_{298}$	$S°_{298}$	$C_p°(T)$								ref
			300 K	400 K	500 K	600 K	800 K	1000 K	1500 K	2000 K	
H	52.10	27.36	4.97	4.97	4.97	4.97	4.97	4.97	4.97	4.97	JANAF[17]
O	59.58	38.47	5.07	5.07	5.07	5.07	5.07	5.07	5.07	5.07	JANAF[17]
O_2	0.0	49.01	6.97	7.24	7.48	7.69	8.03	8.30	8.75	8.89	JANAF[17]
OH	8.89	43.88	7.17	7.08	7.06	7.06	7.15	7.33	7.87	8.36	JPL[18]
HO_2	3.5	54.70	8.42	8.93	9.41	9.86	10.67	11.33	12.39	12.96	JANAF[17]
SO	1.2	53.08	7.23	7.56	7.85	8.09	8.39	8.57	8.76	8.84	b,c
CH_3	35.2	46.30	9.21	10.02	10.79	11.52	12.86	14.02	16.15	17.41	JANAF[17]
SO_2	−70.9	59.30	9.53	10.39	11.13	11.72	12.53	13.02	13.63	13.92	JANAF[17]
CH_2S	28.3	55.14	9.06	10.31	11.48	12.47	14.04	15.22	17.12	18.11	b,c
CH_3O	4.1	54.20	7.95	10.30	12.24	13.85	16.27	17.93	20.34	21.51	THERM[19,20]
CH_3OO	2.2	62.03	13.67	16.18	18.32	20.11	22.87	24.79	27.45	28.77	THERM[19,20]
CH_3S	29.9	57.61	10.71	12.48	14.03	15.35	17.49	19.15	21.86	23.31	b,c
CH_2SO	−10.3	61.12	12.34	14.55	16.28	17.60	19.50	20.83	22.88	23.94	b,c
CH_2O	−26.0	50.90	7.91	9.42	10.69	11.74	13.37	14.51	16.22	18.14	21
SOH	−1.1	57.44	8.85	9.54	10.09	10.52	11.13	11.57	12.38	12.88	c,e
HSO	−7.3	57.74	8.66	9.39	10.05	10.61	11.47	12.07	12.92	13.31	b,c
cyc-(CH_2OS)	7.6	60.28	11.18	13.39	15.26	16.75	18.93	20.44	22.72	23.88	b,c
cyc-(CH_2OS)=O	−39.3	66.75	14.99	17.81	20.08	21.85	24.36	26.05	28.51	29.74	b,c
CH_3SO		62.47	12.17	14.44	16.43	18.08	20.65	22.55	25.54	27.10	c
		5.40	1.49	1.32	1.21	1.15	1.09	1.06	1.02	1.01	IR 1
	−18.95	67.87	13.66	15.76	17.64	19.23	21.74	23.61	26.56	28.11	total, b
anti-CH_3SOO		67.71	14.74	17.31	19.52	21.35	24.15	26.19	29.30	30.97	c
		5.61	1.27	1.16	1.11	1.07	1.04	1.02	1.01	1.00	IR 1
		5.34	3.42	3.07	2.58	2.19	1.70	1.45	1.19	1.10	IR 2
	20.71	78.66	19.43	21.54	23.21	24.61	26.89	28.66	31.49	33.07	total
syn-CH_3SOO		67.17	14.56	17.17	19.41	21.27	24.11	26.19	29.37	30.99	c
		5.61	1.27	1.16	1.11	1.07	1.04	1.02	1.01	1.00	IR 1
		5.34	3.42	3.07	2.58	2.19	1.70	1.45	1.19	1.10	IR 2
	20.16	78.12	19.25	21.40	23.10	24.53	26.85	28.66	31.56	33.09	total, b
CH_3SO_2		67.01	15.44	18.38	20.85	22.85	25.83	27.95	31.21	32.88	c
		4.83	2.09	1.90	1.71	1.55	1.35	1.24	1.11	1.06	IR 1
	−53.65	71.84	17.53	20.28	22.56	24.40	27.18	29.19	32.32	33.94	total, b
C•H_2SO_2H		68.48	16.76	19.57	21.63	23.15	25.32	26.9	29.52	30.99	c
		4.48	1.85	1.70	1.55	1.43	1.28	1.19	1.09	1.05	IR 1
		2.52	2.40	2.33	2.23	2.13	1.93	1.75	1.46	1.30	IR 2
	−27.98	75.48	21.01	23.60	25.41	26.71	28.53	29.85	32.07	33.34	total, b
CH_3OSO		66.03	13.37	15.97	18.33	20.34	23.44	25.69	29.10	30.83	c
		5.67	1.16	1.09	1.06	1.04	1.02	1.01	1.00	1.00	IR 1
		5.83	1.83	1.98	2.02	1.97	1.79	1.62	1.34	1.21	IR 2
	−54.81	77.53	16.36	19.04	21.41	23.35	26.25	28.32	31.44	33.04	total, b
C•H_2SOOH		67.86	15.52	18.09	19.97	21.39	23.45	24.98	27.55	29.01	c
		3.55	2.39	2.24	2.08	1.95	1.74	1.59	1.35	1.23	IR 1
		4.33	3.78	3.87	3.56	3.15	2.45	2.00	1.46	1.26	IR 2
		3.41	1.84	1.76	1.69	1.63	1.52	1.43	1.27	1.18	IR 3
	23.04	79.15	23.53	25.96	27.30	28.11	29.17	30.00	31.64	32.68	total, b
C•$H_2(OH)S$•=O		67.63	13.48	16.36	18.81	20.79	23.73	25.82	29.05	30.74	c
		2.35	1.78	2.14	2.31	2.35	2.23	2.02	1.60	1.37	IR 1
		5.16	2.70	2.79	2.71	2.54	2.14	1.84	1.42	1.24	IR 2
	−54.03	75.14	17.96	21.29	23.84	25.68	28.10	29.67	32.07	33.35	total, b
CH_3SCH_3		55.30	13.61	17.18	20.50	23.39	28.05	31.63	37.38	40.41	e
		4.91	2.02	1.80	1.61	1.47	1.29	1.20	1.09	1.05	e
		4.91	2.02	1.80	1.61	1.47	1.29	1.20	1.09	1.05	e
	−8.94	65.13	17.65	20.79	23.73	26.33	30.64	34.02	39.56	42.51	e
CH_3SSCH_3		70.67	18.73	22.69	26.20	29.18	33.92	37.52	43.29	46.33	e
		5.24	1.77	1.54	1.38	1.28	1.17	1.11	1.05	1.02	e
		5.24	1.77	1.54	1.38	1.28	1.17	1.11	1.05	1.02	e
	−5.76	81.15	22.27	25.76	28.96	31.74	36.25	39.74	45.38	48.37	e
TS1	55.2	79.54	18.00	20.70	23.02	24.92	27.69	29.57	32.28	33.60	b,c
TS2		68.48	15.66	18.13	20.22	21.92	24.54	26.46	29.47	31.04	
		4.83	2.09	1.90	1.71	1.55	1.35	1.24	1.11	1.06	IR 1
	38.0	73.31	17.75	20.03	21.93	23.47	25.89	27.70	30.58	73.31	total, b
TS3	−7.5	71.92	17.36	19.96	22.12	23.86	26.47	28.37	31.37	32.96	b,c
TS4		68.31	15.36	17.65	19.48	20.94	23.16	24.83	27.58	29.08	
		5.67	1.16	1.09	1.06	1.04	1.02	1.01	1.00	1.00	IR 1
		5.83	1.83	1.98	2.02	1.97	1.79	1.62	1.34	1.21	IR 2
	−24.7	79.81	18.35	20.72	22.56	23.95	25.97	27.46	29.92	29.92	total, b
TS5		68.41	13.59	15.74	17.72	19.43	22.15	24.18	27.35	28.98	
		5.61	1.27	1.16	1.11	1.07	1.04	1.02	1.01	1.00	IR 1
		7.20	1.00	1.00	1.00	1.00	0.99	0.99	0.99	0.99	IR 2
	24.9	81.22	15.86	17.90	19.82	21.50	24.18	26.20	29.35	30.97	total, b,c
TS6	32.7	71.25	16.64	19.68	22.22	24.26	27.23	29.24	32.10	33.48	b,c
TS7	22.3	74.84	19.75	22.33	24.19	25.58	27.58	29.06	31.57	33.01	b,c

Multichannel Reaction of Methanethiyl Radical

J. Phys. Chem. A, Vol. 110, No. 21, 2006 **6933**

TABLE 3 (Continued)

species	$\Delta H_f°_{298}$	$S°_{298}$	$C_p°(T)$								ref
			300 K	400 K	500 K	600 K	800 K	1000 K	1500 K	2000 K	
TS8		75.61	18.25	20.83	22.89	24.49	26.85	28.57	31.37	32.91	
		3.55	2.39	2.24	2.08	1.95	1.74	1.59	1.35	1.23	IR 1
	36.8	79.16	20.64	23.07	24.97	26.44	28.59	30.16	32.72	34.14	total, b
TS9		70.01	16.28	18.67	20.67	22.32	24.86	26.74	29.67	31.18	d
		4.83	2.09	1.90	1.71	1.55	1.35	1.24	1.11	1.06	IR 1
	−40.3	74.84	18.37	20.57	22.38	23.87	26.21	27.98	30.78	32.24	total
TS10	−1.1	69.89	17.23	20.51	23.03	24.96	27.69	29.54	32.22	33.54	b,c
TS11		70.22	16.82	19.74	21.82	23.33	25.46	27.00	29.57	31.02	b,c
		2.52	2.40	2.33	2.23	2.13	1.93	1.75	1.46	1.30	IR 1
	−2.7	72.74	19.22	22.07	24.05	25.46	27.39	28.75	31.03	32.32	total
TS12	3.3	70.50	17.37	20.51	22.97	24.88	27.62	29.48	32.20	33.53	b,c
TS13	−3.2	73.94	18.68	21.51	23.58	25.12	27.30	28.87	31.49	32.97	b,c
TS14		71.73	16.88	19.63	21.66	23.18	25.34	26.92	29.54	31.01	
		2.35	1.78	2.14	2.31	2.35	2.23	2.02	1.60	1.37	IR 1
	−1.8	74.08	18.66	21.77	23.97	25.53	27.57	28.94	31.14	32.38	total, b
TS15	20.4	70.88	18.73	21.65	23.96	25.75	28.29	30.00	32.48	33.71	b,c
TS16	58.6	70.13	17.10	20.42	22.98	24.94	27.71	29.57	32.25	33.57	b,c
TS17		72.60	17.92	20.4	22.47	24.18	26.82	28.76	31.73	33.23	d
		5.61	1.27	1.16	1.11	1.07	1.04	1.02	1.01	1.00	IR 1
	−18.95	78.21	19.19	21.56	23.58	25.25	27.86	29.78	32.74	34.23	total, 22
TS18		73.09	17.47	20.08	22.01	23.44	25.5	27.01	29.56	31.01	c
		3.41	1.84	1.76	1.69	1.63	1.52	1.43	1.27	1.18	IR 1
	54.9	76.50	19.31	21.84	23.70	25.07	27.02	28.44	30.83	32.19	total, b
TS19	−6.0	70.19	16.07	19.06	21.64	23.77	26.92	29.06	32.07	33.49	c
TS20	−1.6	71.03	16.76	19.82	22.35	24.37	27.29	29.27	32.10	33.47	c
TS21		67.52	14.79	17.38	19.60	21.42	24.21	26.23	29.37	30.99	
		5.61	1.27	1.16	1.11	1.07	1.04	1.02	1.01	1.00	IR 1
	20.78	73.13	16.06	18.54	20.71	22.49	25.25	27.25	30.38	32.99	total

[a] $\Delta H_f°_{298}$ in kcal/mol, $S°_{298}$ and $C_p°(T)$ in cal/mol·K; temperature range 300−2000 K. [b] $\Delta H_f°_{298}$ is from ref 10. [c] Calculated in this study from B3LYP frequencies using the "SMCPS" program. [d] Calculated in this study from HF/6-31G(d) frequencies using the "SMCPS" program. [e] Unpublished work, $\Delta H_f°_{298}$ is the CBS-QB3 result with the use of isodesmic reactions. IR = internal rotor contribution.

6-31G(d), respectively. The IRC analysis for the TS2′ to TS5 and TS7 to TS21 atom displacement is provided in Supporting Information Figures 1−19. IRC calculations for TS1 ($CH_3S + O_2 \rightarrow CH_2S + HO_2$) and TS6 ($CH_3SOO \rightarrow CH_2S + HO_2$) were reported previously.[10]

3.3. $\Delta H_f°_{298}$ (by Isodesmic Reactions), $S°_{298}$, and $C_p°(T)$ of All Species. Thermochemical parameters are listed in Table 3. Comparisons of calculated enthalpies of formation with the available literature on a number of compounds are illustrated in our previous paper.[10]

3.4. Elementary Reaction Rate Constants. As noted above we find the energy of the transition state structure for the $CH_3S + O_2$ association (TS5) to be ∼ 5.0 kcal/mol below the entrance channel of the reactants and note that this energy is calculated relative to the CH_3SOO adduct. We treat the $CH_3S + O_2$ reaction to TS5 as having no E_a; but being at the energy of the reactants. The preexponential factor is calculated from the TS structure to be 1.2E+12 at 300 K and 1.5E+13 at 2000 K. Dissociation of *anti*-CH_3SOO back to $CH_3S + O_2$ has an E_a of 9.2 kcal/mol with an A factor of 2.2E+13 at 300 K.

All other rate constants for the individual, elementary reactions are determined from the above thermochemical parameters using canonical transition state theory.[11] The results are fit through a temperature range of 300−2000 K and expressed in the form of a three-parameter Arrhenius expression ($A \times T^n \times \exp(E_a(\text{kcal mol}^{-1})/RT)$ and are listed in Table 4.

3.5. Calculated Rate Constants and Comparison with Literature. The elementary rate constants listed in Table 4 are used as input to the multichannel, quantum RRK calculations for $k(E)$ with master equation calculations[11] for pressure dependence to estimate rate constants as a function of temperature and pressure. The bath gas is He. The Lennard-Jones

parameters of 5.6 Å and 650 K are used. The ΔE down is 1000 calories and accounts for collisions with oxygen; an energy bin of 100 calories is used. Rate constant data are shown and explained in the series of figures and tables below for the chemical activation reaction.

Figure 2 illustrates the log of the rate constant for formation of stabilized adduct CH_3SOO (combined *anti-* and *syn-*) vs temperature and pressure. The well depth of this adduct relative to reactants is very shallow, only 9.7 kcal/mol, and this weakly bound adduct dissociates rapidly back to the reactants $CH_3S + O_2$. The discussion below indicates that the adduct is formed rapidly, but it does not mean that the resulting concentration is high nor that is a highly stable final product.

The three lower energy product channels are $CH_2S + HO_2$, $CH_3 + SO_2$, and $CH_3SO + O$. The graphs of rate constants for these channels are also plotted in Figures 2 and 3. These channels show less pressure dependence than the adduct formation; but the rate constants of these three product channels increase with temperature.

$CH_2S + HO_2$ comes from several paths, the most important is molecular elimination of HO_2 from the CH_3SOO adduct via TS6. This barrier is 12.5 kcal/mol at 298 K, only ∼3 kcal/mol higher than the dissociation reaction of CH_3SOO back to $CH_3S + O_2$. The $CH_2S + HO_2$ product set also results from a bimolecular abstraction of a hydrogen atom from CH_3S by O_2; this channel contributes only up to 0.3% (at 2000 K). The least important path to $CH_2S + HO_2$ is the elimination path from $C.H_2SOOH$ which contributes 0.02% (at 2000 K).

All of the $CH_3 + SO_2$ product set comes from the CH_3SOO adduct isomerization through TS2′ to the CH_3SO_2 intermediate. The barrier of this isomerization is 17.8 kcal/mol, 5.3 kcal/mol higher than the competing HO_2 elimination channel, and it also has a tight transition state. The formation of $CH_2S + HO_2$

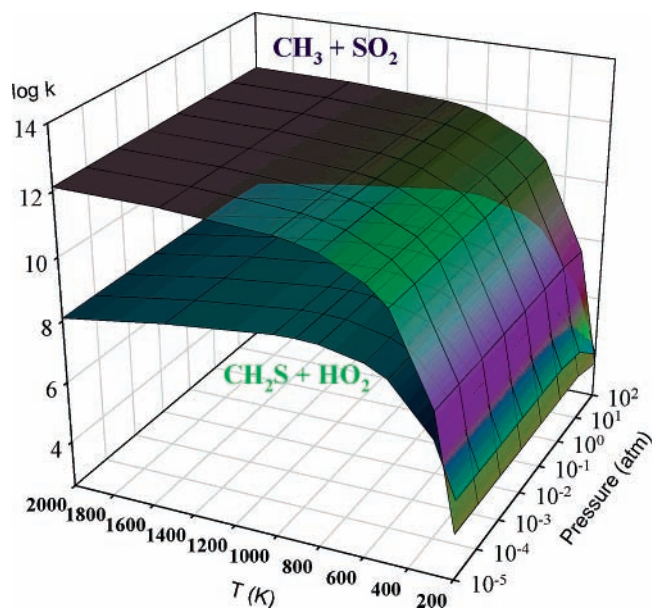**TABLE 4: Input Parameters for $CH_3S + O_2$ System for the Chemical Activation/QRRK-Master Equation Analysis[e,f]**

no.	reactions	$A_\infty{}^a$	n	$E_a{}^b$	$\langle v \rangle^c$
1	$CH_3S + O_2 \rightarrow CH_2S + HO_2$	3.33E+3	2.93	24.6	
5	$CH_3S + O_2 \rightarrow anti\text{-}CH_3SOO$	3.27E+8	1.35	0	398.3 (×7.623), 1611.2 (×3.893),
−5	$anti\text{-}CH_3SOO \rightarrow CH_3S + O_2$	5.21E+14	−0.352	9.2	3349.6 (×2.484)
21	$anti\text{-}CH_3SOO \rightarrow syn\text{-}CH_3SOO$	4.10E+11	0.098	0.07	
−21	$syn\text{-}CH_3SOO \rightarrow anti\text{-}CH_3SOO$	4.63E+11	0.123	0.68	391.3 (×7.377), 1484.4 (×3.619),
2	$syn\text{-}CH_3SOO \rightarrow CH_3SO_2$	3.07E+12	1.677	17.9	3068.3 (×3.004)
16	$syn\text{-}CH_3SOO \rightarrow C.H_2SOOH$	3.49E+7	1.40	37.9	
6	$syn\text{-}CH_3SOO \rightarrow CH_2S + HO_2$	1.92E+8	1.21	12.1	
17	$syn\text{-}CH_3SOO \rightarrow CH_3SO + O$	6.07E+8	1.51	24.3	
−2	$CH_3SO_2 \rightarrow syn\text{-}CH_3SOO$	7.08E+11	0.606	92.0	347.1 (×5.138), 1183.1 (×6.306),
10	$CH_3SO_2 \rightarrow C.H_2SO_2H$	9.12E+8	1.31	52.3	3137.1 (×3.056)
3	$CH_3SO_2 \rightarrow CH_3OSO$	1.20E+11	0.751	46.3	
9	$CH_3SO_2 \rightarrow CH_3 + SO_2$	2.16E+12	0.575	14.8	
−10	$C.H_2SO_2H \rightarrow CH_3SO_2$	1.25E+10	0.579	26.8	348.6 (×7.350), 1038.7 (×4.013),
13	$C.H_2SO_2H \rightarrow CH_2(OH)S^\bullet{=}O$	6.24E+11	0.338	25.0	3407.0 (×2.637)
11	$C.H_2SO_2H \rightarrow CH_2SO + OH$	1.91E+11	0.348	27.1	
−13	$CH_2(OH)S^\bullet{=}O \rightarrow C.H_2SO_2H$	1.02E+11	0.689	50.9	321.2 (×4.323), 990.2 (×7.489),
14	$CH_2(OH)S^\bullet{=}O \rightarrow CH_2SO + OH$	4.77E+10	0.790	53.0	3503.2 (×2.188)
15	$CH_2(OH)S^\bullet{=} \rightarrow cyc\text{-}(COS){=}O + H$	6.48E+7	1.52	73.9	
−3	$CH_3OSO \rightarrow CH_3SO_2$	2.46E+8	1.25	47.2	341.4 (×4.411), 1211.6 (×6.742),
22[d]	$CH_3OSO \rightarrow CH_3O + SO$	4.0E+8	0	57.3	3092.1 (×2.847)
4	$CH_3OSO \rightarrow CH_3 + SO_2$	2.92E+11	0.815	30.5	
19	$CH_3OSO \rightarrow CH_2O + SOH$	2.89E+7	1.403	48.4	
20	$CH_3OSO \rightarrow CH_2O + HSO$	2.44E+6	1.816	53.0	
−16	$C^\bullet H_2SOOH \rightarrow syn\text{-}CH_3SOO$	4.33E+10	0.181	35.5	375.2 (×7.533), 544.1 (×3.516),
7	$C^\bullet H_2SOOH \rightarrow CH_2SO + OH$	6.37E+11	0.087	0	3507.7 (×2.451)
18	$C^\bullet H_2SOOH \rightarrow cyc\text{-}COS + OH$	9.91E+12	−0.180	32.3	
8	$C^\bullet H_2SOOH \rightarrow CH_2S + HO_2$	3.67E+11	0.482	13.7	

[a] A in unit of cm^{-3} mol s. [b] E_a in kcal/mol. [c] Reduced frequency sets, frequency (degeneracy), from CPFIT,[20] in cm^{-1}. [d] Via k_{-22} and microscopic reversibility (MR); $A_{-22} = 5.0E7$ and $E_{a-22} = 0$ from estimation. [e] Lennard-Jones parameters are 5.6 Å and 650 K from ref 23. [f] All rate constants (except k_{22}) are calculated using canonical transition state theory (TST) with TS calculated at CBS-QB3, G3MP2, or G2 levels of theory. Please see discussion in text.
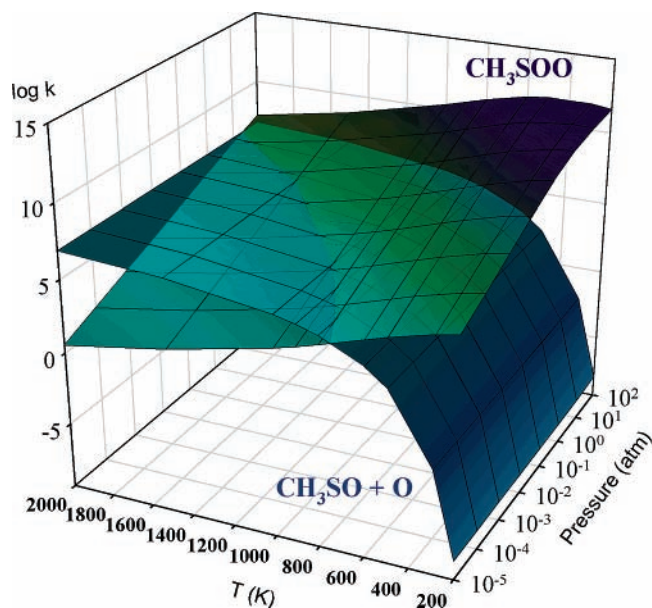
Figure 2. CH_3SOO (*anti-* and *syn-*) and $CH_3SO + O$ formation rate constant (log k) vs temperature and pressure.

Figure 3. Two product sets formation rate constant (log k) vs temperature and pressure.

dominates $CH_3 + SO_2$ over all temperature (300−2000 K) and pressure (10^{-5} to 100 atm) ranges, as illustrated in Figure 3. The difference between these two paths narrows with increased temperature, the ratio of these two rate constants is 5000 at 300 K and decreases to 4 at 2000 K.

The formation of $CH_3SO + O$ shows little pressure dependence but a strong temperature dependence. The comparison in Table 5 shows that this channel has the highest barrier among the three important new products, however it also has the largest A factor of these three paths. It becomes more important at high temperatures, as one would expect.

The total forward rate constant as a function of pressure and temperature is shown in Figure 4. The total forward rate constant is 6.9×10^{11} cm^{-3}/(mol·s) at 300 K and 1 atm, and the dominant species are the two forms of CH_3SOO. The rate constants for the formation of $CH_2S + HO_2$, $CH_3 + SO_2$, and $CH_3SO + O$ are 6.4×10^6, 4.6×10^7, and 4.9×10^{-3} cm^{-3}/(mol·s), respectively, at 300 K and 1 atm.

The calculated rate constants as a function of pressure from QRRK-master equation analysis for the important channels are listed in Table 6.

TABLE 5: Calculated Elementary (High-Pressure Limit) Rate Constants for Selected Products

	syn-$CH_3SOO \rightarrow$ TS2′	syn-$CH_3SOO \rightarrow$ TS6	syn-$CH_3SOO \rightarrow$ TS17
product	$CH_3 + SO_2$ [a]	$CH_2S + HO_2$	$CH_3SO + O$
$E_{a,f}$ (kcal/mol)			
av of 300−2000 K	17.5	12.8	25.4
A_f (s^{-1})			
300 K	5.47E+11	3.89E+11	6.54E+12
400 K	5.99E+11	3.86E+11	8.96E+12
500 K	6.60E+11	4.26E+11	1.19E+13
600 K	7.28E+11	4.95E+11	1.55E+13
800 K	8.84E+11	7.04E+11	2.41E+13
1000 K	1.05E+12	9.93E+11	3.46E+13
1200 K	1.23E+12	1.34E+12	4.64E+13
1500 K	1.47E+12	1.93E+12	6.62E+13
2000 K	1.84E+12	3.04E+12	1.04E+14

[a] Through adduct $CH_3SO_2{}^*$: $CH_3SOO \rightarrow CH_3SO_2{}^* \rightarrow CH_3 + SO_2$.
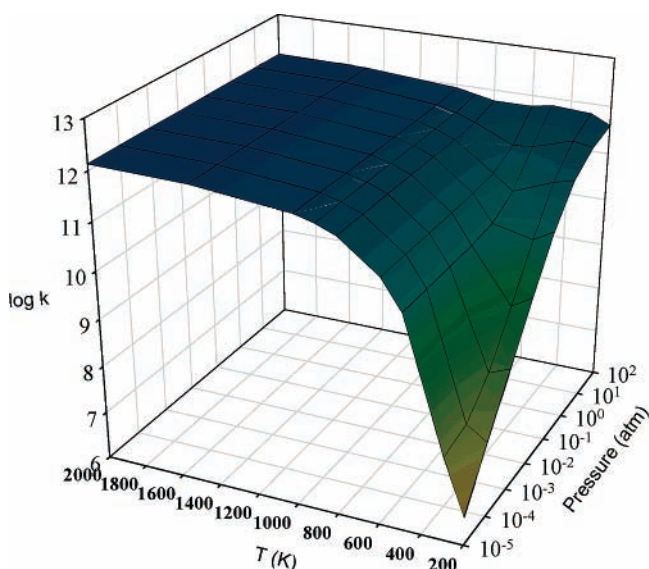

Figure 4. Total forward rate constant (log k) vs temperature and pressure.

The available experimental results, primarily from the review article by Tyndall and Ravishankara[6] are listed in Table 7. The most recent experiment by Turnipseed, Barone, and Ravishankara reports the rate constant of $CH_3S + O_2 \rightarrow CH_3SOO$ to be $(7-18) \times 10^{-14}$ cm^3/(molecule·s), which converts to 4.2×10^{10} to 1.1×10^{11} in cm^3/(mol·s) (units of this study) at 216 and 258 K respectively, and 60−80 Torr of He. Our results estimate the the rate constant of $CH_3S + O_2 \rightarrow CH_3SOO$ at 237 K and 0.1 atm at 3.2×10^{10} cm^3/(mol·s), which close to the lower end of the experimental value.

A small elementary reaction mechanism, for the low temperature early time reactions, is constructed in Table 8. All reactions except R14 are reversible with reverse rate constants calculated from the thermochemical parameters and principles of microscopic reversibility. R3 to R13 in Table 8 of this mechanism are the results of the QRRK-master equation analysis on the $CH_3S + O_2$ system at pressure of 0.1 atm, with only the noted important channels included. We further include a number of reactions in this mechanism relating to reactions of initial products in the experiment of Turnipseed et al.[2] We start the reaction with an initial concentration of CH_3S radical from the data of the experiment, at time zero. As the initial source of CH_3S is CH_3SCH_3 we also add an equal quantity of CH_3 radical. Two CH_3S radicals can combine to dimethyl disulfide without a barrier. R1 and R2 are included in this model to account for these association reactions. The loss of CH_3S radical due to diffusion at the reported rate constant of the experiment is

TABLE 6: Calculated Rate Constants (200−2000 K) for Products vs Pressure

reactions	A	N	E_a (kcal/mol)	pressure (atm)
$CH_3S + O_2 \rightarrow$ anti-CH_3SOO	1.83E+37	−11.0	5.2	1E−5
	1.83E+38	−11.0	5.2	1E−4
	1.84E+39	−11.0	5.2	1E−3
	1.91E+40	−11.0	5.2	1E−2
	2.64E+41	−11.1	5.3	0.1
	9.51E+42	−11.2	5.8	1
	4.54E+44	−11.4	6.8	10
	2.22E+45	−11.3	7.6	100
$CH_3S + O_2 \rightarrow$ syn-CH_3SOO	2.78E+37	−11.1	5.2	1E−5
	2.79E+38	−11.1	5.2	1E−4
	2.80E+39	−11.1	5.2	1E−3
	2.91E+40	−11.1	5.2	1E−2
	3.99E+41	−11.1	5.4	0.1
	1.39E+43	−11.3	5.9	1
	7.00E+44	−11.5	6.8	10
	1.98E+46	−11.6	7.9	100
$CH_3S + O_2 \rightarrow CH_2S + HO_2$	4.71E+24	−4.7	8.3	1E−5
	4.71E+24	−4.7	8.3	1E−4
	4.71E+24	−4.7	8.3	1E−3
	4.71E+24	−4.7	8.3	1E−2
	4.74E+24	−4.7	8.3	0.1
	5.25E+24	−4.7	8.3	1
	2.25E+25	−4.9	8.7	10
	1.54E+27	−5.4	10.0	100
$CH_3S + O_2 \rightarrow CH_3SO + O$	5.25E+13	−1.5	16.9	1E−5
	5.25E+13	−1.5	16.9	1E−4
	5.25E+13	−1.5	16.9	1E−3
	5.25E+13	−1.5	16.9	1E−2
	5.24E+13	−1.5	16.9	0.1
	5.19E+13	−1.5	16.9	1
	4.66E+13	−1.5	16.8	10
	2.49E+13	−1.4	16.7	100
$CH_3S + O_2 \rightarrow CH_3 + SO_2$	9.44E+25	−3.8	12.3	1E−5
	9.44E+25	−3.8	12.3	1E−4
	9.44E+25	−3.8	12.3	1E−3
	9.45E+25	−3.8	12.3	1E−2
	9.47E+25	−3.8	12.3	0.1
	9.77E+25	−3.8	12.3	1
	1.44E+26	−3.9	12.4	10
	7.31E+27	−4.4	13.2	100

included and assumed irreversible (R14). The methyl radicals from photochemical dissociation of the dimethyl sulfide (in the experiment) are active in this O_2 rich environment and the reactions R15 and R22−24 are amended. The barrierless radical−radical associations of CH_3S with CH_3SOO and CH_3OO form energized adducts ($CH_3SOOCH_3{}^*$ or $CH_3SOOSCH_3{}^*$) with up to 70 kcal/mol excess energy and these energized adducts undergo exothermic dissociation of the weak peroxide bonds to oxy radicals, reactions R17 to R21. As an example:

TABLE 7: Literature Data on CH₃S + O₂ Reaction System[a]

k (cm³/(molecule s))	experimental method	ref
2E−13	product study	Hatakayama and Akimoto[24]
3E−17	product study	Grosjean[25]
>1.5E−16	product study	Balla and Heicklen[26]
<2E−17	LP/LIF	Balla et al.[4]
<2E−16	LP/LIF	Black and Jusinski[27]
<2E−18	LP/LIF	Tyndall and Ravishankara[3]
(7−18)E−14	LP/LIF, CH₃SOO	Turnipseed et al.[2]
5.4E−14	computational chem	this study

[a] Conditions: ∼ 0.1 atm and room temperature to 200 K.

TABLE 8: Kinetic Model for CH₃S + O₂ System (0.1 atm, 200−2000 K)

reactions	A^a	n	$E_a{}^b$	ref
$CH_3SCH_3 \rightarrow CH_3 + CH_3S$ (R1)	4.89E+37	−7.05	78.14	c
$CH_3SSCH_2 \rightarrow 2CH_3S$ (R2)	7.10E+39	−7.75	70.33	d
$CH_3S + O_2 \rightarrow anti\text{-}CH_3SOO$ (R3)	2.64E+41	−11.07	5.29	e
$CH_3S + O_2 \rightarrow syn\text{-}CH_3SOO$ (R4)	3.99E+41	−11.13	5.36	e
$CH_3S + O_2 \rightarrow CH_2S + HO_2$ (R5)	4.74E+24	−4.67	8.29	e
$CH_3S + O_2 \rightarrow CH_3SO + O$ (R6)	5.24E+13	−1.50	16.85	e
$CH_3S + O_2 \rightarrow CH_3SO_2$ (R7)	3.44E+12	−5.94	14.14	e
$CH_3S + O_2 \rightarrow CH_3 + SO_2$ (R8)	9.47E+25	−3.80	12.33	e
$anti\text{-}CH_3SOO \rightarrow syn\text{-}CH_3SOO$ (R9)	2.49E+46	−10.06	80.48	e
$syn\text{-}CH_3SOO \rightarrow CH_2S + HO_2$ (R10)	7.86E+44	−10.86	79.95	e
$syn\text{-}CH_3SOO \rightarrow CH_3SO + O$ (R11)	2.80E+44	−10.55	79.95	e
$syn\text{-}CH_3SOO \rightarrow CH_3SO_2$ (R12)	4.67E+48	−10.40	79.95	e
$CH_3SO_2 \rightarrow CH_3 + SO_2$ (R13)	2.31E+00	3.39	9.58	e
$CH_3S \rightarrow CH_3S(INV)$ (irreversible) (R14)	120	0	0	f
$CH_3 + O_2 \rightarrow CH_3OO$ (R15)	1.2E+12	0	0	g
$CH_3S + CH_3OO \rightarrow CH_3SO + CH_3O$ (R16)	1.0E+13	0	0	g
$CH_3S + anti\text{-}CH_3SOO \rightarrow 2CH_3SO$ (R17)	2.5E+12	0	0	g
$CH_3S + syn\text{-}CH_3SOO \rightarrow 2CH_3SO$ (R18)	2.5E+12	0	0	g
$anti\text{-}CH_3SOO + anti\text{-}CH_3SOO \rightarrow 2CH_3SO + O_2$ (R19)	3.4E+10	0	−1.5	h
$anti\text{-}CH_3SOO + syn\text{-}CH_3SOO \rightarrow 2CH_3SO + O_2$ (R20)	3.4E+10	0	−1.5	h
$syn\text{-}CH_3SOO + syn\text{-}CH_3SOO \rightarrow 2CH_3SO + O_2$ (R21)	3.4E+10	0	−1.5	h
$CH_3 + CH_3 \rightarrow C_2H_6$ (R22)	4.31E+33	−6.65	4.64	i
$CH_3 + CH_3OO \rightarrow 2CH_3O$ (R23)	1.0E+13	0	0	g
$CH_3OO + CH_3OO \rightarrow 2CH_3O + O_2$ (R24)	5.5E+10	0	−0.42	h

[a] A in unit of cm⁻³, mol, and s. [b] E_a in kcal/mol. [c] High-pressure limit k is estimated as $A = 2E+16$, $E_a = 73.3$, and then used as inputs of QRRK-master equation analysis. The results are shown here. [d] High-pressure limit k is estimated as $A = 2E+16$, $E_a = 65.0$, and then used as inputs of QRRK-master equation analysis. The results are shown here. [e] From QRRK-master equation analysis, input are in Table 4. [f] CH₃S (INV) is the invisible CH₃S: the loss of CH₃S is due to diffusion.[2] [g] Estimations. [h] Reference 28. [i] High-pressure limit k is estimated as $A = 3E13$, $E_a = 0$, and then used as inputs of QRRK-master equation analysis, the results are shown here.

$$CH_3S + CH_3SOO \leftrightarrow CH_3SOOSCH_3{}^* \leftrightarrow 2\,CH_3SO,$$
$$\Delta H_{rxn} = -90 \text{ kcal/mol}$$

(We note an additional exothermicty results from rearrangement of the two CH₃S−O• radicals to the more stable electronic form CH₃S•(=O)).

If the energy is partitioned equally in the two CH₃SO products, then each CH₃SO will have sufficient chemical activation energy (ΔH_{rxn}) to dissociate to H₂O + HC•=S or CH₂S + OH before collisional stabilization occurs. (Barriers for these last two reactions are not included in the thermochemical estimate).

The CHEMKIN II mechanism integrator is used to model the three reaction conditions of Turnipseed et al.[2] where O₂ concentrations are 1.29E+16, 3.48E+16, or 4.6E+16 molecules/cm³. The temperature is 216 K and the pressure is 80 Torr of He as used in their experiment. The profiles of CH₃S radical from our mechanism are compared with the experiments in Figure 5. Our mechanism overestimates the loss of CH₃S radicals at all three [O₂] conditions, since our overall CH₃S + O₂ well depth is lower, 9.7 vs 11.2. We feel this result is acceptable for this initial quantum RRK chemical activation analysis and will move to RRKM analysis for improved accuracy.

The product profiles from the Chemkin run are shown in Figure 6 for conditions of 216K and 0.1 atm of He, with [O₂] = 1.3 × 10¹⁶ molecules/cm⁻³. The major species in the system are CH₃OO and CH₃SOO. CH₃SOO starts to dominate CH₃S radical after 1 ms. The CH₃SOO concentration is 10 times higher than dimethyl disulfide before 1 ms, 100 times higher than CH₃SO, and about 4 orders of magnitude higher than CH₂S + HO₂, which is the most important unimolecular (forward) reaction from the CH₃SOO adduct.

4. Summary

Thermochemistry, kinetic parameters, and a potential energy surface for the CH₃S• + O₂ reaction system are studied using density functional, ab initio, and composite methods in computational chemistry. The analysis extends into thermochemistry and potential surfaces for the CH₃ + SO₂ and CH₂=S=O + OH association reactions and unimolecular dissociation of CH₃SO₂, and CH₃OSO. Kinetics of the CH₃S• + O₂ system are analyzed in detail and compared with experimental studies from the literature.

The well depth for the CH₃S• + ³O₂ reaction to CH₃SOO• adduct is very shallow at 9.7 kcal/mol. Three exit channels from the CH₃SOO• adduct to CH₂S + HO₂, CH₃ + SO₂, and CH₃SO + O are found to have low reaction barriers; but all of these
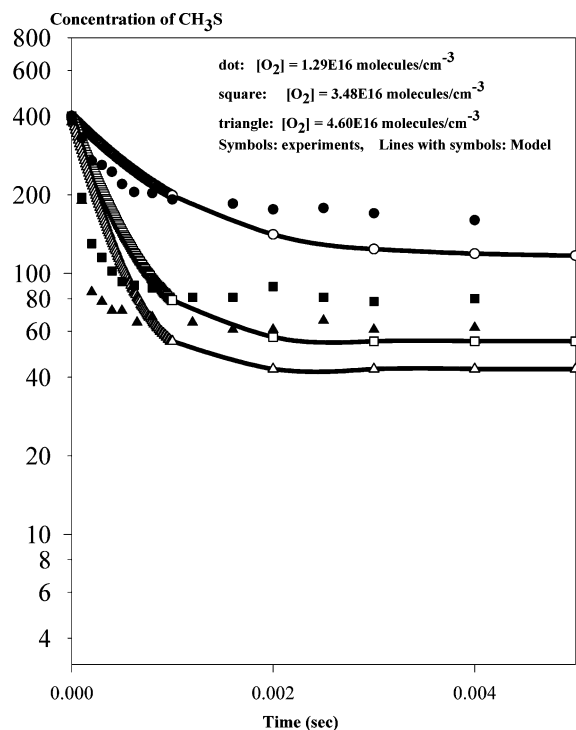
Multichannel Reaction of Methanethiyl Radical

J. Phys. Chem. A, Vol. 110, No. 21, 2006 **6937**

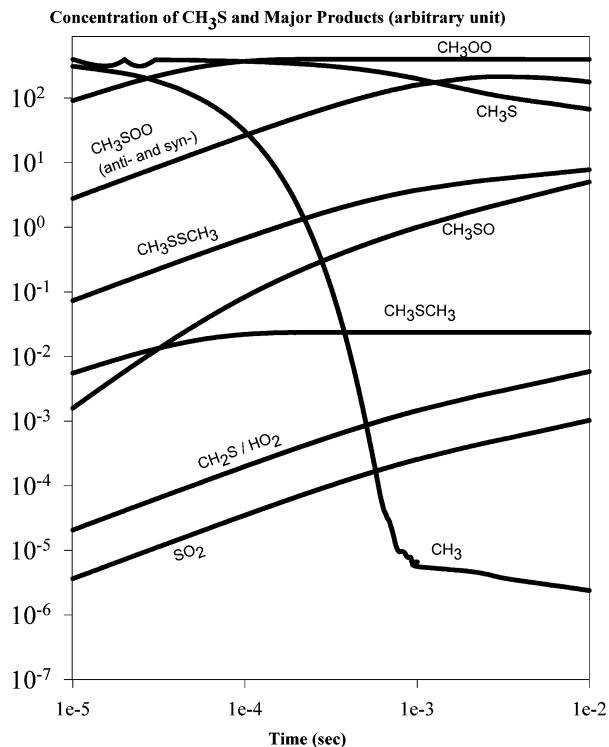**Figure 5.** Comparison of model with the experiment data for the decay of CH_3S radical at 216 K and 80 Torr of He.

Figure 6. Major species at 216 K and 80 Torr of He, $[O_2] = 1.29E+16$ molecules/cm^{-3}.

barriers are slightly higher than reverse reaction of CH_3SOO to $CH_3S^\bullet + O_2$. All transition states in this weakly bound CH_3S-OO system including adduct formation/dissociation are tight, on a comparative basis. Rate constants to these channels are estimated at conditions of temperatures and pressure. The CH_3SOO adduct primarily dissociates back to reactants $CH_3S^\bullet + O_2$, with fractions of both the chemically activated CH_3SOO^* and stabilized CH_3SOO adducts reacting to products over barriers that are several kcal/mol higher than reaction back to

reactants. Rate constants and thermochemistry of the CH_3SOO adduct and transition states are in reasonable agreement with the experimental data in the literature. The G3MP2 and CBS-QB3 composite methods are recommended for sulfur − oxygen hydrocarbon systems and show significantly better agreement with literature than the density functional methods used in this study.

Supporting Information Available: Plots of internal reaction coordinates (IRC), which are important for verifying reaction paths and are included in the SM for reactions TS2′ through TS5 and TS7 through TS21. This material is available free of charge via the Internet at http://pubs.acs.org.

References and Notes

(1) Charlson, R. J.; Lovelock, J. E.; Andreae, M. O.; Warren, S. G. *Nature* **1987**, *326*, 655.
(2) Turnipseed, A. A.; Barone, S. B.; Ravishankara, A. R. *J. Phys. Chem.* **1992**, *96*, 7502.
(3) Tyndall, G. S.; Ravishankara, A. R. *J. Phys. Chem.* **1989**, *93*, 2426.
(4) Balla, R. J.; Nelson, H. H.; McDonald, J. R. *Chem. Phys.* **1986**, *109*, 101.
(5) Barnes, I.; Bastian, V.; Becker, K. H.; Niki, H. *Chem. Phys. Lett.* **1987**, *140*, 451.
(6) Tyndall, G. S.; Ravishankara, A. R. *Int. J. Chem. Kinet.* **1991**, *23*, 483.
(7) Butkovskaya, N. I.; Barnes, I. *NATO Sci. Ser. 4, Earth Environ. Sci.* **2002**, *16*, 147.
(8) Frank, A. J.; Turecek, F. *J. Phys. Chem. A* **1999**, *103*, 5348.
(9) Yin, F.; Grosjean, D.; Seinfeld, J. H. *J. Atmos. Chem.* **1990**, *11*, 309.
(10) Zhu, L.; Bozzelli, J. W. *J. Mol. Struct. (THEOCHEM)* **2005**, *728*, 147.
(11) Sheng, C. Ph.D. Dissertation. Department of Chemical Engineering, New Jersey Institute of Technology, Newark, NJ, 2002.
(12) Lay, T. H.; Krasnoperov, L. N.; Venanzi, C. A.; Bozzelli, J. W. *J. Phys. Chem.* **1996**, *100*, 8240.
(13) Shokhirev, N. V. University of Arizona, Tempe, Arizona, http://www.chem.arizona.edu/faculty/walk/nikolai/programs.html#programs.
(14) Zhu, L.; Bozzelli, J. W. *Chem. Phys. Lett.* **2002**, *357*, 65.
(15) Kee, R. J.; Rupley, F. M.; Miller, J. A. *Chemkin-II: A Fortran Chemical Kinetics Package for the Analysis of Gas-Phase Chemical Kinetics*; reprint ed.; Sandia National Lab.: Livermore, CA, 1992.
(16) Wang, S. K.; Zhang, Q. Z.; Cao, C. B.; Gu, Y. S. *Acta Chim. Sinica* **2002**, *60*, 432.
(17) Stull, D. R.; Prophet, H. *JANAF Thermochemical Tables*, 2nd ed. (NSRDS−NBS 37); U. S. Government Printing Office: Washington, DC, 1970.
(18) Sander, S. P.; Friedl, R. R.; Ravishankara, A. R.; Golden, D. M.; Kolb, C. E.; Kurylo, M. J.; Huie, R. E.; Orkin, V. L.; Molina, M. J.; Moortgat, G. K.; Finlayson-Pitts, B. J. *Chemical Kinetics and Photochemical Data for Use in Atmospheric Studies*; Evaluation Number 14, JPL Publication 02-25; JPL: Pasadena, CA, Feb. 1, 2003; can be downloaded from http://jpldataeval.jpl.nasa.gov/download.html.
(19) Ritter, E. R.; Bozzelli, J. W. *Int. J. Chem. Kinet.* **1991**, *23*, 767.
(20) (a) Bozzelli, J. W.; Ritter, E.; Dean, A. M. *Int. J. Chem. Kinet.* **1997**, *29*, 161. (b) Ritter, E. R. *J. Chem. Info. Comput. Sci.* **1991**, *31*, 400.
(21) da Silva, G. R.; Bozzelli, J. W. Thermodynamic and ab initio analysis of the controversial enthalpy of formation of formaldehyde. *ChemPhysChem.* **2006**, *7*, 1119.
(22) Jin, Fei.; Master Thesis. Department of Chemistry and Environmental Science, New Jersey Institute of Technology, Newark, NJ, 2003.
(23) Reid, R. C.; Prausnitz, J. M.; Polling, B. E. *Properties of Gases and Liquids*; 4th ed.; McGraw-Hill: New York, 1989.
(24) Hatakeyama, S.; Akimoto *J. Phys. Chem.* **1983**, *87*, 2387.
(25) Grosjean, D. *Environ. Sci. Technol.* **1984**, *18*, 460.
(26) Balla, R. J.; Heicklen, J. *J. Photochem.* **1985**, *29*, 297.
(27) Black, G.; Jusinski, L. E. *J. Chem. Soc., Faraday Trans. 2:* **1986**, *82*, 2143.
(28) Rosado-Reyes, C. M.; Francisco, J. S.; Szente, J. J.; Maricq, M. M.; Østergaard, L. F. *J. Phys. Chem. A* **2005**, *109*, 10940.